ACS Chemical Neuroscience

pubs.acs.org/chemneuro Research Article

In Vitro Diagnosis and Visualization of Cerebral Ischemia/Reperfusion Injury in Rats and Protective Effects of Ferulic Acid by Raman Biospectroscopy and Machine Learning

Mingying Liu,[∞] Ju Mu,[∞] Wan Gong, Kena Zhang, Maoyun Yuan, Yizhi Song, Bei Li, Naifu Jin, Wenjing Zhang, and Dayi Zhang*

Cite This: *ACS Chem. Neurosci.* 2023, 14, 159−169 Read Online

ACCESS | Metrics & More | Article Recommendations | Supporting Information

ABSTRACT: Ischemic stroke is a major cause of mortality with complicated pathophysiological mechanisms, and hematoxylin and eosin (HE) staining is a histochemical diagnosis technique heavily relying on subjective observation. In this study, we developed a noninvasive assay using Raman spectroscopy for *in vitro* diagnosis and visualization of cerebral ischemia/reperfusion injury and protective effects of ferulic acid. By establishing a middle cerebral artery occlusion (MCAO) model in Sprague-Dawley male rats, we found effective interventions by ferulic acid using the neurological function score and HE staining. Raman spectra of neuronal and neuroglial cells exhibited significant intensity changes of protein, nucleotide, lipid, and carbohydrate at 780, 814, 1002, 1012, 1176, 1224, 1402, 1520, 1586, 1614, and 1752 cm^{-1}. Cluster vector analysis highlighted the alterations at 1002, 1080, 1298, 1430, 1478, 1508, 1586, and 1676 cm^{-1}. To evaluate the levels of neuron injury and intervention performance, a random forest model was developed on Raman spectral data and achieved satisfactory accuracy (0.9846), sensitivity (0.9679−0.9932), and specificity (0.9945−0.9989), ranking peaks around 1002 cm^{-1} as key fingerprint for classification. Spectral phenylalanine-to-tryptophan ratio was the biomarker to visualize neuronal injury and intervention performance of ferulic acid with a resolution of 1 μm. Our results unravel the biochemical changes in neuronal cells with cerebral ischemia/reperfusion injury and ferulic acid treatment, and prove Raman spectroscopy coupled with machine learning as a power tool to classify neuron viability and evaluate the intervention performance in pharmacological research.

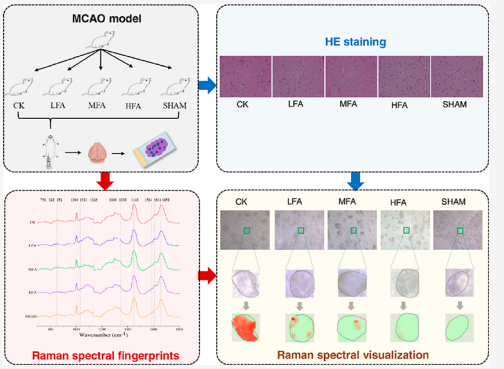

KEYWORDS: *Ischemic stroke, vibrational spectroscopy, machine learning*

1. INTRODUCTION

Ischemic stroke is the major cause of mortality leading to acquired disability.[1] Recanalization therapies are the most widely adopted clinical treatments intending to replenish nutrients and oxygen and remove toxic metabolites.[2] However, ischemic stroke has complicated pathophysiological mechanisms[3] and narrow therapeutic window,[4] and recanalization strategies may therefore worsen tissue injuries and cause inflammatory responses accompanying restoration of blood flow.[3] Oxidative stress and blood−brain barrier damage in cerebral ischemia also exacerbate the inflammatory response exhibiting the elevations of immune cells and inflammation related metabolites.[3] Immune cells are deemed to contribute to infarct growth and maturation in animal models of transient middle cerebral artery occlusion (tMCAO) mimicking human stroke treated with recanalization.[5]

Ferulic acid (4-hydroxy-3-methoxycinnamic acid) is an important active ingredient isolated from traditional Chinese medicine such as *Ligusticum striatum*.[6] As ferulic acid is not stable, sodium ferulate is more often used in clinical practice for treating heart and head blood-vessel disease and exerts protective effects against hypoxia/ischemia-induced cell injury in brain.[7] Pharmacological studies have suggested the critical roles of ferulic acid in vasodilatation, antiplatelet activity, and free radical scavenging.[8] Both ferulic acid and sodium ferulate are reported to perform neuroprotection by countering with glutamate-induced apoptosis[9] and overexpressing heme oxygenase, exhibiting significant neuroprotective effects on ROS and glucose oxidase related oxidative damage.[10−12] Besides, ferulic acid can also exert neuroprotective effects during psychosocial stress exhibiting an enhancement of long-term memory.[6,12] Therefore, there is an increasing attention on ferulic acid and sodium ferulate as a promising neuroprotective

Received: October 8, 2022
Accepted: November 29, 2022
Published: December 14, 2022

agent for the treatment of cerebral ischemia due to their significant effects of anti-inflammation, antioxidative stress, angiogenesis, and neurogenesis contributing to improvement of neurological functions on ischemic stroke.[13,14]

Hematoxylin and eosin (HE) staining is as an essential histochemical technique for analyzing pathogenesis, informing lesions and formulating the histopathological diagnosis.[15] HE staining discloses abundant structural information on well-fixed cells, displaying a broad range of cytoplasmic, nucleic, and extracellular matrix features.[16] However, HE staining relies on proper specimen processing and is limited by chemical regents.[17] The lesions of HE staining are also incompatible with further clinical purposes such as immunofluorescence.[17] In addition, microscopic elucidation heavily relies on subjective observation, leading to the possibility of false-negative results.[15] Therefore, there is an urgent need to develop an alternative, objective and noninvasive technique based on early stage biochemical changes rather than morphologies of tissues or cells.

In the recent years, vibrational spectroscopy has gained increasing attentions due to its advantages in providing chemical and structural information on biological samples, exhibiting great potential in clinical diagnosis.[18−20] Raman spectroscopy has been extensively used for diagnosing cancer,[20] disease,[19] and illicit drugs.[21] Raman spectral signatures of amyloid β aggregation in neural tissues provide a detailed image of amyloid plaques in brain and are potential biomarkers for noninvasive and early diagnosis of Alzheimer's disease.[22] However, no study has used Raman spectroscopy to diagnose neuronal injury caused by ischemic reperfusion or evaluate the neuroprotective effects of ferulic acid. It is therefore of urgency to assess the feasibility of Raman spectroscopy in ischemic stroke studies and establish biospectral databases of neuronal cells as guidance for other brain diseases.

In this study, we established a MCAO model in Sprague-Dawley (SD) male rats to mimic ischemic reperfusion injury and ferulic acid treatments of different doses. With the aid of neurological scoring and HE staining, a novel and robust analytical method was developed using Raman spectroscopy coupled with multivariate analysis and machine learning. We aimed to discriminate key Raman peaks responding to ischemic reperfusion injury and ferulic acid intervention, evaluate the levels of injury and intervention of neurons by elucidating spectral features, and visualize the neurological deficits for clinical purposes. Our findings will offer clues for noninvasively assessing the neuroprotective effects of ferulic acid and provide foundations for the pharmacological screening of potential drugs treating stroke.

2. RESULTS AND DISCUSSION

2.1. Improved Neurological Deficit by Ferulic Acid from Neurological Behavior Assessment. We observed the effects of interventions based on the neurological function scores, indicating a protective effect of ferulic acid against stroke (Figure 1). On day 1, SD rats in CK group receiving MCAO showed a significant increase in neurological deficit (2.667 ± 0.5) than SHAM group ($p < 0.01$). Ferulic acid groups exhibited no dramatic amelioration compared with CK group. On day 3, ferulic acid group with high dose of 100 mg/kg (HFA group) ameliorated neurological deficits (1.778 ± 0.441) during ischemia versus CK group ($p < 0.01$). On day 7, ferulic acid groups with medium (MFA group, 1.556 ± 0.527, $p < 0.05$) and high dose (HFA group, 1.111 ± 0.601, $p < 0.01$) exhibited the alleviation effects of neurological deficits during ischemia versus CK group. However, no significant difference was found in the low dose group (LFA, 1.778 ± 0.441, $p > 0.05$) compared to CK group.

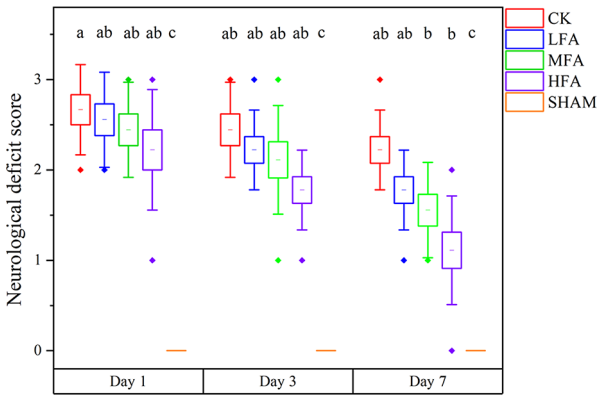

Figure 1. Neurological deficit score of rats after ischemia−reperfusion. CK represents model group and SHAM refers to sham-operation group. LFA, MFA, and HFA represent treatments with low (25 mg/kg), medium (50 mg/kg), and high (100 mg/kg) dose of sodium ferulate, respectively.

2.2. Alleviated Morphological Changes after Cerebral Ischemia/Reperfusion Injury by Ferulic Acid from HE Staining. Morphological changes induced by cerebral ischemia/reperfusion injury were assessed by HE staining (Figure 2), and there were no obvious autolysis compared to other HE staining results in our laboratory. Seven days after ischemia/reperfusion, neuronal cells in SHAM group were neatly arranged with a clear structure, normal shape, and round nucleus (Figure 2A). However, neurons in CK group exhibited a disorganized cell arrangement and nuclear condensation, and immune cells appeared (Figure 2B). Compared with CK groups, ferulic acid treatment displayed the alleviation of cell injury (Figure 2C−E). Especially in HFA group, the symptoms of living cell swelling, intercellular space broadening, and nuclear constriction were remarkably alleviated. Our results confirmed that ferulic acid interventions achieved neuroprotective functions during ischemia/reperfusion injury.

2.3. Neuron Discrimination As Revealed by Raman Spectra. Raman spectra of neuronal and neuroglial cells from five groups generated 10 sets of key data recording the information on major biomolecules, as listed in Figure 3A,B (for details see Table S1). Characteristic peaks related to nucleotides were located at 570 cm^{-1} (DNA), 728 cm^{-1} (adenine), 780 cm^{-1} (cytosine, urine, and thymine), 1256 cm^{-1} (adenine and cytosine), 1338 cm^{-1} (adenine and guanine), and 1584 cm^{-1} (adenine and guanine). Phosphate−sugar backbone vibrations displayed the peak at 1090 cm^{-1}. Lipid peaks were observed at 828 cm^{-1} (O−P−O asymmetric stretch), 984 cm^{-1} (=CH bend), 1064 cm^{-1} (C−C skeletal), 1156 cm^{-1} (C−C stretch), and 1300 cm^{-1} (C−H deformation). The peaks of carbohydrates were 938 (C−O−C ring) and 1030 and 1338 cm^{-1} (CH_2 deformation). Intense peaks of proteins included 758 cm^{-1} (symmetric ring breathing in tryptophan), 1002 and 1584 cm^{-1} (L-phenylalanine), 1268 and 1558 cm^{-1} (N−H bend and C−N stretch in amide III), 1338 and 1448 cm^{-1} (CH_2 deformation), and 1658 cm^{-1} (stretching vibrations of C=O in amide I). Some other key peaks arose from 620 cm^{-1} (C−C twist in phenylalanine), 642

https://doi.org/10.1021/acschemneuro.2c00612
ACS Chem. Neurosci. 2023, 14, 159−169

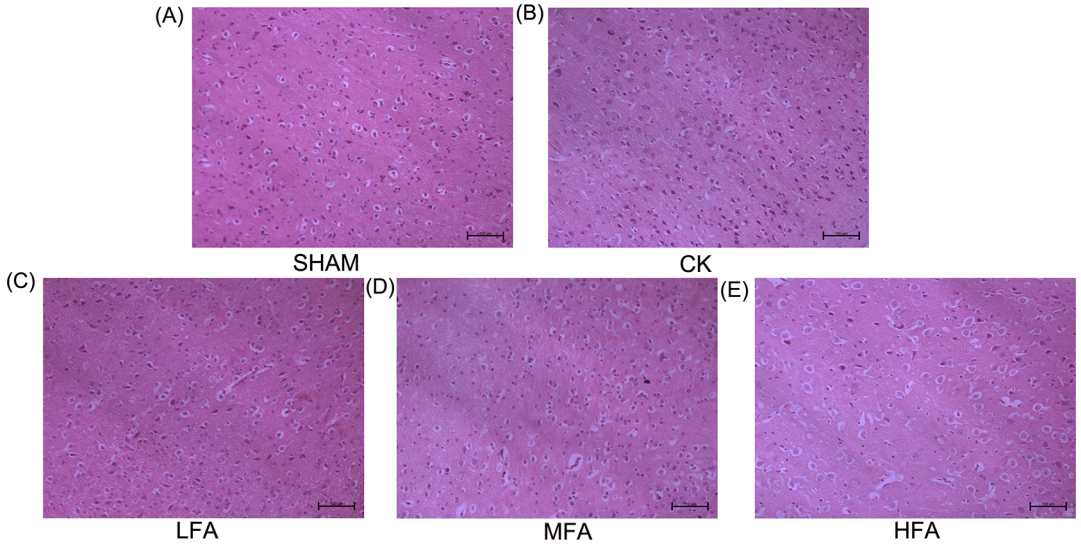

Figure 2. HE staining for the effects of ferulic acid on pathomorphological changes of rat brain after cerebral ischemia−reperfusion (×400). CK represents the model group, and SHAM refers to the sham-operation group. LFA, MFA, and HFA represent treatments with low (25 mg/kg), medium (50 mg/kg), and high (100 mg/kg) dose of sodium ferulate, respectively.

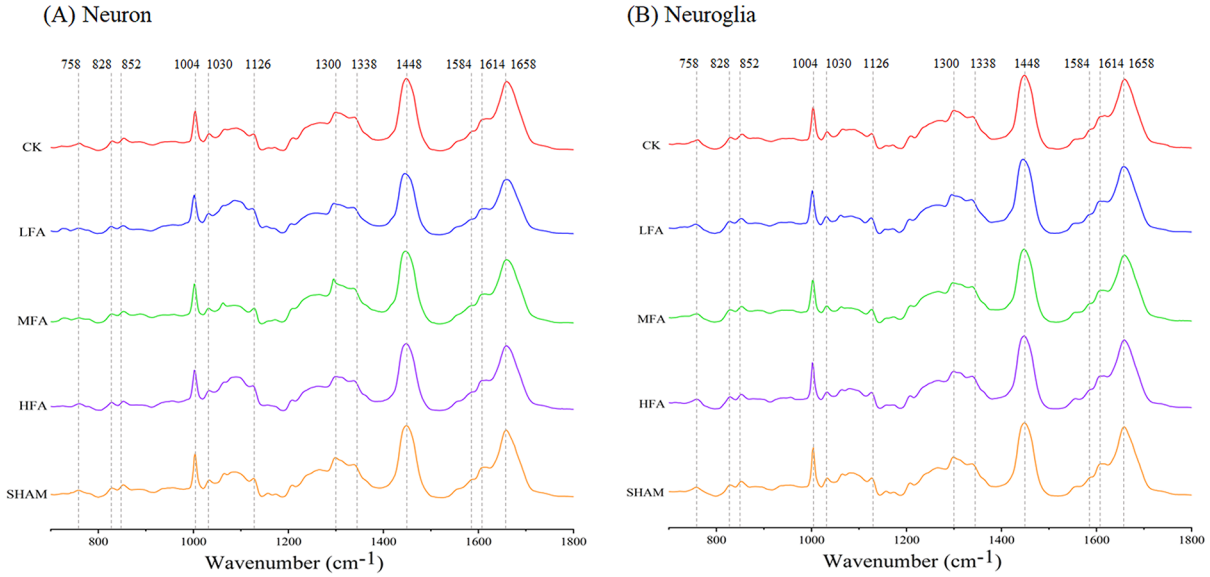

Figure 3. Raman spectra of neuron (A) and neuroglia (B) in different groups. CK represents the model group, and SHAM refers to the sham-operation group. LFA, MFA, and HFA represent treatments with low (25 mg/kg), medium (50 mg/kg), and high (100 mg/kg) dose of sodium ferulate, respectively.

cm^{-1} (C−C twist in tyrosine), 852 cm^{-1} (C−C stretch in proline, ring breathing in tyrosine), 1030 cm^{-1} (C−H bend in phenylalanine), and 1126 cm^{-1} (C−N stretch of protein).

Raman spectra among different groups had very tiny differences with obvious spectral overlaps and nonevident intensity changes, exerting difficulties for classification. We therefore analyzed the spectral alterations with significant intensity change ($p < 0.05$) between key groups (Figure S1). Here, the spectra regions marked in red and blue indicated significant altered Raman peaks between SHAM and CK ($p < 0.05$) and nonsignificant altered ones between SHAM and HFA groups ($p > 0.05$), respectively. The spectral regions meeting both criteria included 780 cm^{-1} (thymine, cytosine, and uracil), 814 cm^{-1} (not annotated, close to peaks representing O−P−O asymmetric stretch), 998−1004 cm^{-1} (C−C skeletal in phenylalanine), 1012 cm^{-1} (not annotated, close to peaks of C−C skeletal in phenylalanine), 1176 cm^{-1} (C−H bend in tyrosine), 1224 cm^{-1} (not annotated, close to peaks of C−C_6H_5 stretch in phenylalanine and CH_2 twist in tryptophan), 1402 cm^{-1} (not annotated, close to peaks of CH_2 deformation), 1520 cm^{-1} (not annotated, close to peaks representing N−H bend and C−N stretch in amide III), 1584 cm^{-1} (adenine, guanine, phenylalanine), 1614 cm^{-1} (C═C in tryptophan and tyrosine), and 1752 cm^{-1} (not annotated). Among them, the intensities of peaks at 780 cm^{-1} (Figure 4A), 1002 cm^{-1} (Figure 4B), and 1176 cm^{-1} (Figure 4C) exhibited an elevation with sodium ferulate dose, whereas the peaks of 1586 cm^{-1} (Figure 4E) and 1614 cm^{-1} (Figure 4F) were opposite. For 1222 cm^{-1}, its intensities declined with sodium ferulate dose but were different between CK and LFA groups (Figure 4D and Figure S5).

https://doi.org/10.1021/acschemneuro.2c00612
ACS Chem. Neurosci. 2023, 14, 159−169

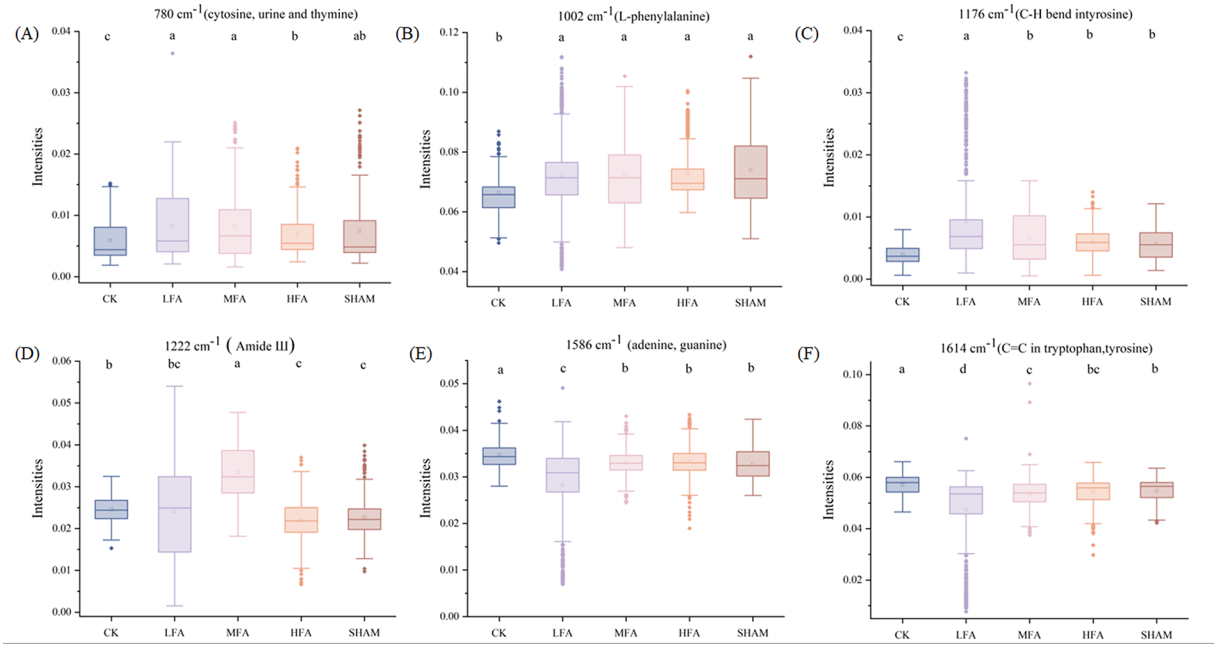

Figure 4. Raman peak intensities of neuronal cells among different groups: (A) 780 cm^{-1} for cytosine, urine, and thymine (nucleotides); (B) 1002 cm^{-1} for C−C skeletal in phenylalanine; (C) 1176 cm^{-1} for C−H bend in tyrosine; (D) 1222 cm^{-1} (not annotated); (E) 1586 cm^{-1} for adenine, guanine, phenylalanine; (F) 1614 cm^{-1} for C═C in tryptophan, tyrosine. CK represents the model group, and SHAM refers to the sham-operation group. LFA, MFA, and HFA represent treatments with low (25 mg/kg), medium (50 mg/kg), and high (100 mg/kg) dose of sodium ferulate, respectively.

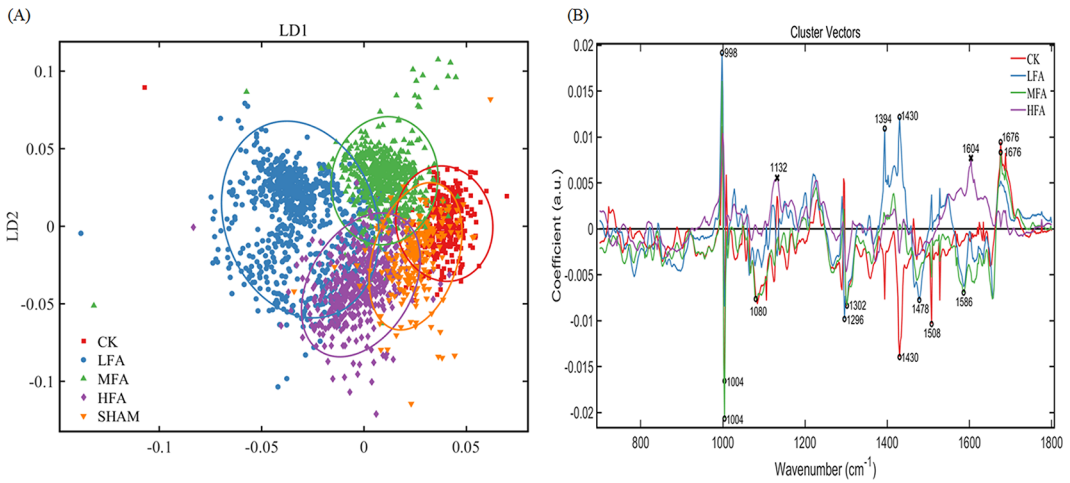

Figure 5. PCA score plot (A) and cluster vectors (B) of Raman spectra of neurons from different groups. CK represents the model group, and SHAM refers to the sham-operation group. LFA, MFA, and HFA represent treatments with low (25 mg/kg), medium (50 mg/kg), and high (100 mg/kg) dose of sodium ferulate respectively.

Direct comparison of peak intensities was complicated and time-consuming. Therefore, multivariate analysis was conducted to discriminate unique features among all recorded biochemical variations to classify neurons across groups. PCA-LDA algorithm extracted the key biochemical variations among five groups and classified neurons (Figure 5A) and neuroglia (Figure S3) treated with sodium ferulate. However, PCA-LDA score plots illustrated no obvious segregation of five groups, and cluster vector analysis was performed to reveal more information (Figures 5 and S4). As illustrated in Figure 5B, seven cluster vectors were highlighted and responsible for segregation, including 998−1004 cm^{-1} (C−C skeletal in phenylalanine), 1080 cm^{-1} (C−N stretch), 1298 cm^{-1} (C−H deformation), 1430 cm^{-1} (CH_2 deformation), 1478 cm^{-1} (CH_2 deformation), 1508 cm^{-1} (not annotated), 1586 cm^{-1} (adenine, guanine, and phenylalanine), and 1676 cm^{-1} (C═O stretch in amide I). These discriminating regions had obvious peak shift (1002 cm^{-1}, Figure S2A), different shapes (1080 cm^{-1}, Figure S2B; 1298 cm^{-1}, Figure, S2C), or different slopes (1430 cm^{-1}, Figure S2D; 1478 cm^{-1}, Figure S2E; 1508 cm^{-1}, Figure S2F; 1586 cm^{-1}, Figure S2G; 1676 cm^{-1}, Figure S2H).

2.4. Classification by RF Models. The RF model based on Raman spectra was constructed and satisfactorily classified the levels of injury and intervention of neurons. The relationships between error and tree numbers became smooth when ntree was 400 and maintained stability until ntree was 500 (Figure 6A). Thus, ntree = 500 and mtry = 6 were set. Generally, OOB error rate was 1.79%, hinting at a high

https://doi.org/10.1021/acschemneuro.2c00612
ACS Chem. Neurosci. 2023, 14, 159−169

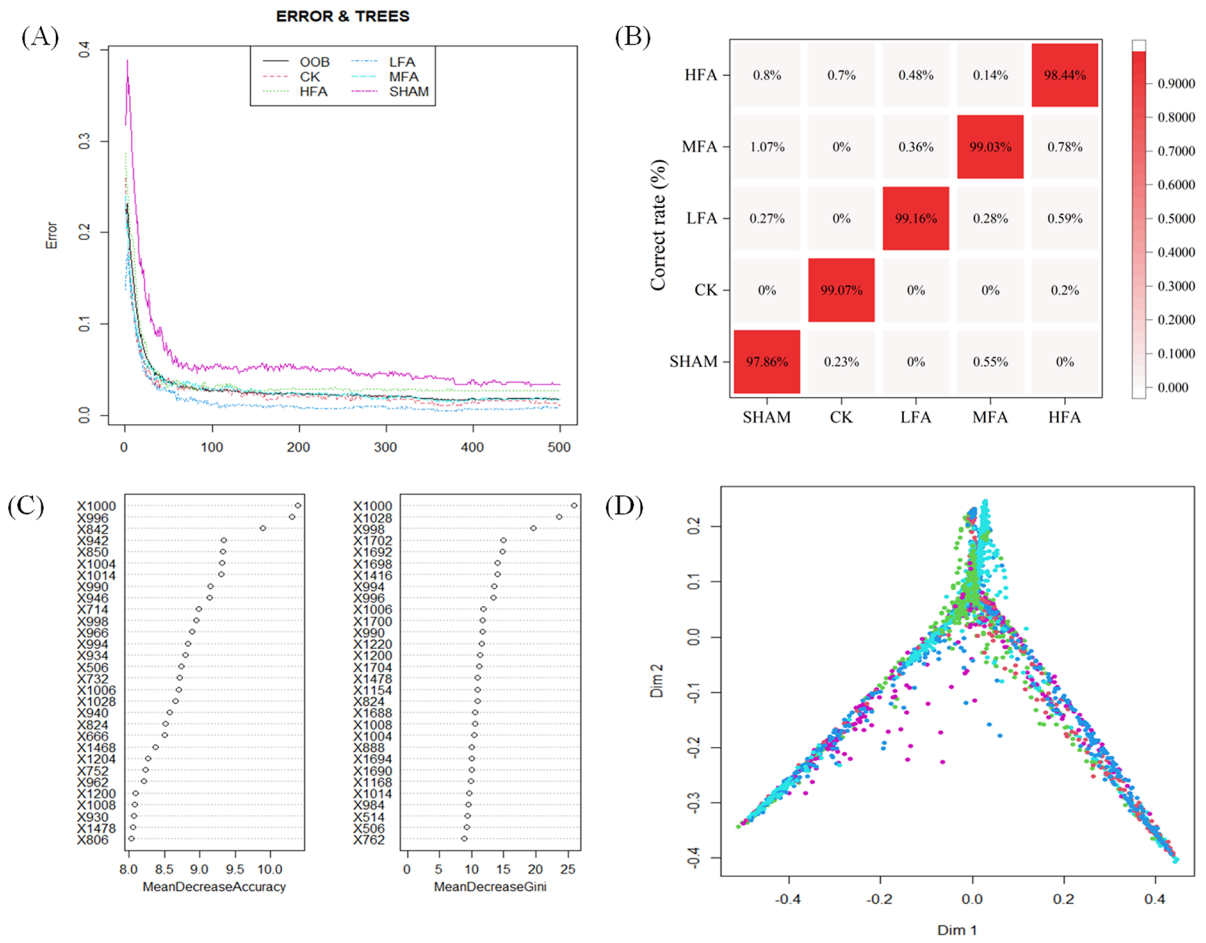

Figure 6. Random forest model for evaluating the levels of injury and intervention of neurons. (A) Relationships between error and tree numbers. (B) Accuracy of established five-class RF model. (C) MeanDecreaseGini and MeanDecreaseAccuracy of the variant importance. The top 20 vibrational peaks are listed. (D) MDsplot visualizing RF model. CK represents the model group, and SHAM refers to the sham-operation group. LFA, MFA, and HFA represent treatments with low (25 mg/kg), medium (50 mg/kg), and high (100 mg/kg) dose of sodium ferulate, respectively.

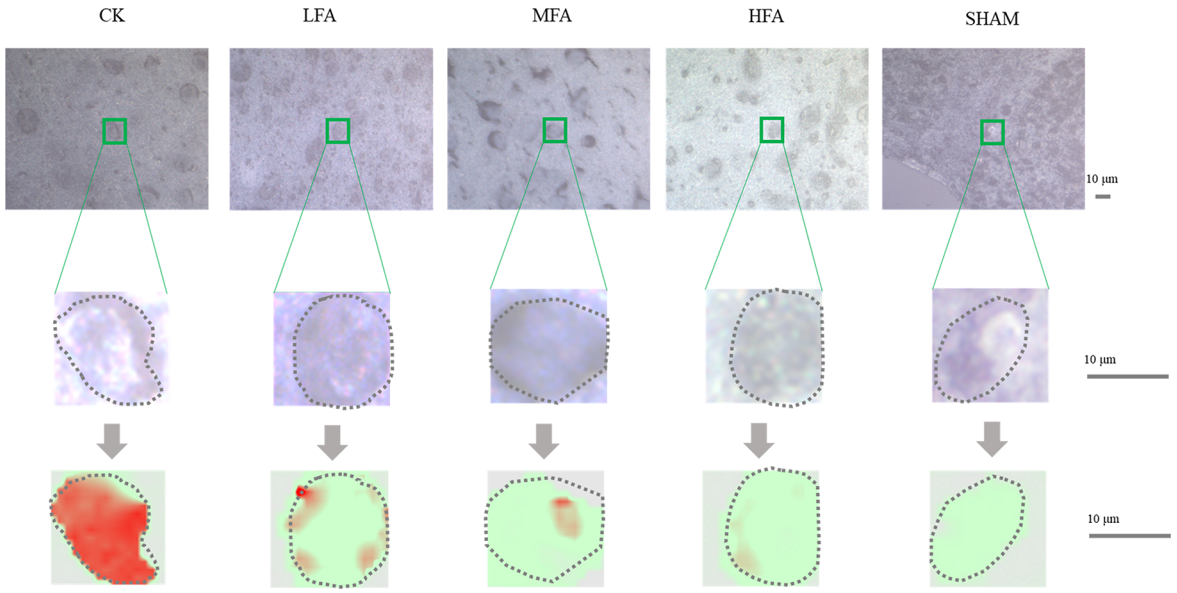

Figure 7. Mapping of neurons and neuroglia among different groups based on key Raman alterations. CK represents the model group, and SHAM refers to the sham-operation group. LFA, MFA, and HFA represent treatments with low (25 mg/kg), medium (50 mg/kg), and high (100 mg/kg) dose of sodium ferulate, respectively. Data are 226 spectra from each group (20 subfigures, 10 for white/black image, 10 for Raman spectra based on phenylalanine-to-tryptophan ratios).

https://doi.org/10.1021/acschemneuro.2c00612
ACS Chem. Neurosci. 2023, 14, 159−169

prediction accuracy. The value of class.error was 1.111%, 2.669%, 0.862%, 1.794%, and 3.381% for the classification of CK, HFA, LFA, MFA, and SHAM groups, respectively. Overall, the accuracy of the established RF model was 0.9846 (Figure 6B, κ = 0.9803). Sensitivity was 0.9932, 0.9679, 0.9885, 0.9871, and 0.9854 for CK, HFA, MFA, LFA, and SHAM groups, respectively. Specificity was 0.9989, 0.9965, 0.9949, 0.9945, and 0.9956 for CK, HFA, MFA, LFA, and SHAM groups, respectively. The accuracy of RF model could also be assessed through the values representing multiclass area under the curve, which was 0.8303, 0.7943, 0.853, 0.7983, and 0.8064 for the classification of CK, HFA, MFA, LFA, and SHAM groups, respectively. The variant importance was calculated by MeanDecreaseGini and MeanDecreaseAccuracy (details see Table S2), and 1000 cm^{-1} was ranked as the most important peak for predictive classification (Figure 6C). The other key variables were 998, 842, 1004, 1416, and 1692 cm^{-1} (Figure 6C), the majority of which represented lipids and proteins. Model visualization showed that the test samples belonging to the same group were clustered together and immensely distributed and <20 spots were scattered separately, hinting at the reliability and accuracy of the developed model (Figure 6D).

Another RF classification model was also established to classify both cell types (neuron and neuroglia) and cell viability across groups (Figure S6). However, OOB error rate was 18.84% and the accuracy ranged from 63.83% to 91.56% for each group. The false classification was mainly caused by the classification in CK and SHAM groups. Both neuronal and neuroglial cells were vigorous in CK group, whereas they were all rigidly damaged in SHAM group.

2.5. Neuron Mapping and Diagnosis by Raman Spectra. Based on cluster vector analysis, neurons in CK group exhibited higher spectral phenylalanine-to-tryptophan ratios (peak intensities at 1002 cm^{-1} to peak intensities at 1614 cm^{-1}), and their intensities were much lower in SHAM groups. Thus, spectral phenylalanine-to-tryptophan ratio was used to *in vitro* visualize neuronal viabilities with a resolution of 1 μm (Figure 7). Raman spectral mapping fitted well with white/black images that all neurons exhibited the same shape. It was obvious that in CK group, the majority of neuronal cells exhibited high phenylalanine-to-tryptophan ratios (marked in red), whereas they were of low phenylalanine-to-tryptophan ratio (marked in green) in SHAM group. As for LFA, MFA, and HFA groups, the color gradients from red to green suggested the increasing intervention performance of ferulic acid with dosage. It is worth noting that neuronal cells showed uneven distribution of phenylalanine-to-tryptophan ratios, and there were some hotspots representing severe neuron injuries in CK, LFA, MFA, and HFA groups. These data suggested that Raman spectral visualization could not only diagnose the levels of neuron injury and intervention performance but also highlight the sites of injury on neuronal cells.

Ischemic stroke is the second single most frequent cause of death for older people, leading to permanent disability and dementia.[23] Due to the remaining substantial neurological deficits in patients,[24,25] cerebral ischemia/reperfusion injury is regarded as a major threat to human health and survival with a high morbidity.[26] Therefore, neuroprotection that reduces neuronal and glial cell damages under the threshold of symptom manifestation is an important index for the evaluation of treatment strategies and clinical outcomes of patients with acute stroke.[24] Currently, the evaluation of neuroprotective effects relies heavily on HE staining and clinical experience. It is therefore important to develop an objective and noninvasive approach based on early stage biochemical changes rather than morphologies of tissues or cells. Raman spectroscopy is a fingerprint spectrum produced by the interactions between light and matter, highlighting the chemical identity and state of biomolecules via their distinctive scattering properties at the molecular level.[27] It has been proposed as a potential noninvasive tool to detect early oxidative stress in neurodegenerative diseases.[28] This work applied Raman spectroscopy to diagnose the levels of injury and intervention of neurons in MACO model rats. Through multivariate analysis of Raman spectral data and RF model, our results established the comprehensive links between biospectra of neuronal cells and their physiological functions, implying a powerful and noninvasive approach to diagnose the cerebral ischemia/reperfusion injury in rats and evaluate the protective effects of ferulic acid.

In this study, neurological examination results confirmed obvious damages in ischemia/reperfusion group receiving MACO with increasing neurological deficit scores, indicating the successful model construction (Figure 1). Intervention with ferulic acid showed a significant improvement of alleviated neurobehavioral symptoms supported by the morphological results (Figure 2). The morphological observations proved the variances among groups depicted by cell arrangements, cell shape, and nucleus status. Ferulic acid extracted from traditional Chinese herbal medicines has been found to counteract oxidative stress[12,13] and perform the cytoprotective effects in case of damage caused by neurotoxicants.[11] For instance, ferulic acid is reported to reduce glutamate-evoked apoptotic morphology of cultured cortical neurons incubated with glutamate.[9] It also exerts neuroprotection in human neuroblastoma cells exposed to neurotoxin trimethyltin through the up-regulation of the heme oxygenase-1 and biliverdin reductase system.[11] In addition to these antioxidant effects, ferulic acid could maintain the homeostasis by modulating cellular autophagy, closely related to processing and elimination of misfolded proteins.[29] These findings support the effects of ferulic acid in counteracting cerebral ischemia injury and provide a possibility of ferulic acid application in neurodegenerative diseases characterized by cognitive impairment. However, besides examining the neurological behaviors, more direct and accurate proof should characterize the neuroprotective mechanisms of ferulic acid. Therefore, the neuroprotection of ferulic acid requires assessment from molecular biochemical changes instead of morphological status. Hence, it is vital to investigate the changes in biochemical components involved in neuronal cell death, and more such precise and microcosmic findings contribute to the identification of potential protective components and the development of effective drugs and therapy strategies.

Raman biospectra of neuron and neuroglia in different groups (Figure 3) illustrated a mixture of distinct biomolecules. The annotated fingerprints represented major cellular molecules including protein, nucleotides, lipid, and carbohydrates (Table S1). The main protein peaks implied peptide vibrational modes, including C−C stretch, C−N stretch, C═O stretch, S−S stretch, N−H bend, and C−H bend. Additionally, biomarkers of protein secondary conformation were identified, including amide III (1268 and 1558 cm^{-1}) and amide I (1655−1698 cm^{-1}). Amide I vibration is associated

https://doi.org/10.1021/acschemneuro.2c00612
ACS Chem. Neurosci. 2023, 14, 159−169

with C═O stretching in the peptide backbone and is subjected to different restoring forces in the α-helix and β-sheet.[30] Amide III is a complex vibration mode obtained from the sum of N−H bending and C−N stretching and is influenced by (C)CαH bending motion.[31] Previous studies have reported that the postischemic aggregation of ubiquitin, small ubiquitin-related modifier, and ribosomes is closely related to post-translational protein modifications that potentially function in neuron protection.[32,33] However, cerebral ischemia could also induce the aggregation of neurodegeneration-related disease proteins which may lead to neuronal dysfunction and death.[34] Regardless of the processes, a thriving protein metabolism occurs in neurons, displaying a homeostatic imbalance and candidate discriminating biomarkers. In addition, the key alterations also included phenylalanine aromatic ring side chains (620, 1004, 1030, 1208, and 1584 cm^{-1}), tyrosine (642, 758, 1176, and 1614 cm^{-1}), and proline (852 cm^{-1}). Amino acids are the basic units of proteins and perform critical roles in cell signaling, biosynthesis, transportation, and key metabolic pathways. Altered levels of amino acids are closely related to many diseases including neurological diseases, liver diseases, and stroke.[35] Our results suggested that Raman spectroscopy is a powerful tool to identify neuronal damage in the imbalanced biological disease network caused by stroke by distinguishing the biomarkers of protein metabolism.

Besides protein metabolism, other biomolecules such as nucleic acids, fatty acids, lipids, and low-density lipoprotein have also been reported to alter in the serum and plasma of cerebral ischemia patients.[3] In this study, some peaks of nucleic acids, lipids, and carbohydrates were altered. Characteristic peaks implying nucleic acids were 728 cm^{-1} (adenine), 780 cm^{-1} (thymine, cytosine, and uracil), 1256 cm^{-1} (adenine and cytosine), 1338 cm^{-1} (CH_2 deformation of adenine and guanine), and 1588 cm^{-1} (adenine and guanine). These results hinted at the involvement of DNA replication and RNA expression in the protective effects of cerebral ischemic,[26] consistent with some previous studies reporting the altered gene expression profiles in TLR4/MYD88 inflammatory signaling, HRAS/RAF1 neurotrophic signaling, and hypermethylated N^6-methyladenosine modification pathways, which might be the key mechanisms involved in secondary injury following cerebral ischemia−reperfusion.[36,37] Our findings offered spectral evidence for the alterations of key DNA and RNA in cerebral ischemia.

Lipids are constituted of different members and serve as energy storage, signaling molecules, and membrane component contributing to tissue physiology. Detrimental changes in lipid metabolism and excess accumulation of lipids contribute to a variety of metabolic disorders resulting in a lack of axon regeneration and poor neurological outcome after central nervous system trauma and disease.[38] Our findings highlighted some vibrational alterations related to lipids, including C−C stretch (1064 and 1156 cm^{-1}), C−C−N^+ stretch (888 cm^{-1}), C═C stretch (1655−1698 cm^{-1}), and ═CH bend (984 cm^{-1}) and O−P−O asymmetric stretch (828 cm^{-1}) (Figure 3 and Table S1). Besides, the peaks of carbohydrates like C−O−C ring (888 and 938 cm^{-1}) and CH_2 deformation (1338 cm^{-1}) also significantly altered. These results evidenced the feasibility of using Raman spectra to diagnose the biochemical changes of damaged neurons. A study has applied Raman microspectroscopy to assess the chemical composition of a hippocampal neuron coculture undergoing oxidative stress and found the time-dependent changes of nucleic acid peaks.[28] Our study for the first time identified some key vibrational fingerprints exhibiting changes in lipid metabolism from neuronal cells as candidate biomarkers.

We also focused on the representative fingerprints discriminating the different viabilities of neurons. Here, Raman spectra of neuronal and neuroglial cells in different groups were not segregated in PCA-LDA score plot (Figure 5A), possibly attributing to tiny cellular changes of neuronal cells in the cerebral ischemia/reperfusion injury. We thus further analyzed predominant alterations to distinguish the key biomarkers representing biochemical changes using intensity change and cluster vector analysis. By comparing the regions with significant intensity changes (780, 814, 1002, 1012, 1176, 1224, 1402, 1520, 1584, 1614, and 1752 cm^{-1}) and cluster vectors (1002, 1080, 1298, 1430, 1478, 1508, 1586, and 1676 cm^{-1}), we find two key peaks of 1002 cm^{-1} (phenylalanine) and 1586 cm^{-1} (phenylalanine and purines) highlighted by both methods, suggesting they were predominant biomarkers of neuronal injury and intervention.

Besides discriminating the unique fingerprints, Raman spectroscopy also successfully evaluated the pharmacological effects, and a more robust classification model was therefore required. Here, the developed RF model achieved satisfactory accuracy, sensitivity, and specificity (Figure 6), capable of assessing the levels of neuronal injury and intervention by ferulic acid. The most dependent peak was around 1002 cm^{-1} of phenylalanine, meeting well with the results of cluster vector analysis (Figure 5B). Metabolic pathways of two aromatic amino acids tyrosine and phenylalanine are reported to correlate, and phenylalanine hydroxylase is the key enzyme converting phenylalanine to tyrosine, which is an essential precursor in the brain for the monoamine neurotransmitter serotonin and catecholamines that may increase due to excitation in the sympathetic nervous system during an acute ischemic stroke.[39] Amino acid metabolism is heavily involved in the pathophysiology of acute brain ischemia,[40] and amino acids or their derivatives can serve as blood biomarkers for the stroke diagnosis.[41,42] A study investigated the therapeutic effects of a Chinese medicine (BuChang NaoXinTong) on reversing cerebral ischemia and found an imbalanced amino acid−key enzyme−protein network.[43] Particularly, some amino acid biomarkers such as phenylalanine, tyrosine, and tryptophan are found to significantly change in MCAO group,[43] and a decreasing phenylalanine level is observed in the stroke group compared with sham operated male Wistar rats.[40] The disturbance of aromatic amino acid metabolism can affect energy metabolism by compromising Krebs cycle functioning and decreasing key enzyme activities enrolled in biological oxidation. These will lead to oxidative stress,[44] which is a vital factor responsible for most of the ischemia−reperfusion injury and thus causing brain apoptosis, autophagy, and necrosis.[45] In this study, the identified vibrational biomarker of 1002 cm^{-1} representing phenylalanine by three algorithms served as a unique fingerprint discriminating neurons with different viabilities and hinted at the intervention mechanisms of ferulic acid.

Biospectral imaging has been enormously applied in biological and biomedical studies to visualize the inherent features with the aid of chemometrics methods.[46] Here, we *in vitro* visualized neuronal cell viabilities by using the spectral phenylalanine-to-tryptophan ratio (1002 cm^{-1} to 1614 cm^{-1}) with a resolution of 1 μm (Figure 7). The two vibrational biomarkers were selected because 1002 cm^{-1} (L-phenyl-

https://doi.org/10.1021/acschemneuro.2c00612
ACS Chem. Neurosci. 2023, 14, 159−169

alanine) and 1614 cm^{-1} (C═C in tryptophan and tyrosine) were highlighted by both multivariate analysis and RF models, representing the altered amino acid metabolisms during acute brain ischemia.[40] Raman imaging has been widely used for living biological cells,[47] including univariate approach using individual biomarkers of deoxyadenosine triphosphate for neuron cells[48] or cyclopropane fatty acids for yeasts[49] and multivariate approaches using multiple key peaks for blood cells.[50] However, no previous studies have attempted to visualize neuronal injury caused by ischemic reperfusion and neuroprotective effects. Our study used a classification-based Raman imaging coupled with machine learning (RF model) to successfully visualize the injury of the whole neuronal cells and even the sites of injury, proving the feasibility of using Raman spectral imaging for diagnosing cerebral ischemia/reperfusion injury and screening potential drugs with neuroprotective effects.

3. MATERIALS AND METHODS

3.1. Animals and Drugs. In total, 45 SD rats (250−280 g each) were bred in the Medical Animal Experimentation Center of Zhejiang Chinese Medical University and maintained under a 12 h/12 h light/dark cycle with free access to food and water. Sodium ferulate was purchased from Yuanye Medical Pharmaceutical Co. Ltd. (Shanghai, China). All animal treating procedures were carried out in strict accordance with the Institutional Animal Care and Use Committee of China and followed the regional Animal Ethics Committee of Zhejiang Chinese Medical University.

3.2. MCAO Model. The MCAO model was established as described previously.[51] Briefly, male SD rats were anesthetized with 4% chloral hydrate (1 mL in 100 g) intraperitoneally and placed on a heating pad to maintain the body temperature at 36.5−37.5 °C. The right common carotid artery (CCA) was isolated and exposed first, followed by the external carotid artery (ECA) and internal carotid artery (ICA). Then, a nylon monofilament approximately 0.24 mm in diameter with a blunt white tip was inserted through ECA into ICA to block the origin of middle cerebral artery (MCA) until the slight resistance was felt. Cerebral ischemia was maintained for 2 h, and the suture was put off slowly to restore arterial blood flow for 72 h reperfusion. After the operation, all rats were placed in a suitable environment to maintain normal body temperature. The sham-operated rats underwent the same surgical procedures as MCAO rats without inserting a filament.

3.3. Drug Administration and Groups. Sodium ferulate was dissolved in saline (0.9%), and rats were administered intravenously once a day after operation. SD male rats were randomly divided into 5 groups of 9 rats each, comprising model group (CK), low ferulic acid dosage group (LFA), medium ferulic acid dosage group (MFA), high ferulic acid dosage group (HFA), and sham-operation group (SHAM). A dose of 0.9% saline was administered to CK and SHAM groups. The dosage of sodium ferulate was 25, 50, and 100 mg/kg for LFA, MFA, and HFA groups, respectively.

3.4. Neurological Deficit Evaluation. Neurologic examinations were performed to assess the neurological deficits of five groups in a blind manner on 1-, 3- and 7-day postischemia. The neurologic functions were scored on a five-point scale as in ref 52: score of 0 for no neurologic deficit; score of 1 for a mild focal neurologic deficit showing failure to extend left forepaw fully; score of 2 for a moderate focal neurologic deficit showing circling to the left; score of 3 for a severe focal deficit exhibiting the falling to the left; score of 4 for rats not able walk spontaneously and with a depressed level of consciousness.

3.5. HE Staining. HE staining was used to microscopically observe the morphologies and pathologies of brain cells by staining the slices. All MCAO rats were immediately executed after perfusion with precooled saline followed by 4% paraformaldehyde to avoid autolysis, and the whole process was done within 25 min. Then, the brains were sampled and fixed with 4% paraformaldehyde and stored at 4 °C. After 24 h, the fixed brain tissues were embedded in paraffin and cut into a series of 5 μm thick sections for storage. Before staining, the brain slices were first deparaffinized to remove paraffin wax using xylene and hydrated using anhydrous/diluted alcohols (95% and 70%). Then, HE staining was performed by rinsing the slides in H_2O, dehydrated twice with 95% and 100% alcohol, respectively, followed with two times exchange of methanol. The slices were added with one or two drops of mounting medium and covered with a coverslip. The images were taken under 40× objective lens (Zeiss, Germany) using microscope Imager A2 (Zeiss, Germany).

3.6. Raman Biospectroscopic Acquisition and Analysis. Paraffin-fixed brain tissues were cut into a series of 5 μm thick sections, placed onto BaF_2 slides, and dewaxed to avoid the spectral interference of paraffin. Raman spectra[53] were acquired using a confocal Raman spectrometer P300 (HOOKE Instruments Ltd., China) equipped with an integrated microscope and a motorized *XYZ* stage. Tissue visualization and spectral acquisition were achieved through a 50×/NA 0.5 objective (HOOKE Instruments Ltd., China). Raman scattering was excited with a 532 nm laser diode and detected with a −75 °C air-cooled charge coupled detector (CCD). Raman spectral measurements with grating 1200 g/mm resulted in a spectral resolution of ∼2 cm^{-1} over spectral range from 350 to 2000 cm^{-1}. The acquisition time was 15 s, and the exposure power was 20 mW. Raman mapping was conducted in an area of 16 μm × 16 μm on each slide, and the step was 1 μm (a total of 256 spectra for each mapping area and at least 200 spectra were extracted for mapping after RF model evaluation). For each group, three individual slides were analyzed as biological replicates, and at least 3 areas were randomly selected for mapping.

3.7. Data Analysis. Raman spectral data preprocessing and classification were carried out within MATLAB (MathWorks, Natick, USA) implemented with an in-house developed IRootLab toolbox (http://trevisanj.github.io/irootlab/).[54] Spectral data with background noise or nonbiological variability eliminated were truncated to the biological region (2000−500 cm^{-1}), wavelet was denoised, polynomial was baseline corrected, and vector was normalized, following the standard procedure in Raman spectral analysis of biological samples to generate noise-free spectra with conventional appearance. The resulting data set was first mean-centered and then applied to the cross-validated (*k*-fold = 10 and leave-one-out to avoid overfitting) principal component analysis (PCA) followed by linear discriminant analysis (LDA) to discriminate the differences. All classification models were validated using 10% of the samples in a test set. This unsupervised method can extract a few important principal components (PCs) responsible for the majority of variance from the spectral data set. Cluster vector analysis was conducted to visualize the subtle difference and discriminate specific Raman bands closely associated with neuron status. SHAM was set to be the "index of class to be the origin".

To evaluate the levels of injury and intervention of neurons by retaining the most effective features from spectral data, we built a multivariant classification model by random forest (RF) algorithm, which is a multiclassifier algorithm based on ensemble learning and composed of hundreds of trees grown through a bootstrap sample. Each node selected by each tree corresponded with a random variables subset which serves as candidates to search the best split for the node. To construct RF model, the normalized spectral data were imported to RStudio (version 3.4.1) and calculated by "randomForest" package. All data (4116 spectra) were first divided into training and test sets (3:1), and the category of different neuron groups was deemed as the factor with various spectral peaks as the variables. The further split of the entire training data set generated two groups (1:3), model training data set (771 spectra) for model construction and model validation data set (2315 spectra) for the model evaluation exporting results as out-of-bag (OOB) data. A multivariable classification model was constructed using the optimized references (ntree value of 500, mtry value of 6). The variable importance sort was performed to rank the essential variables and export the confusion matrix and training and testing votes for each

https://doi.org/10.1021/acschemneuro.2c00612
ACS Chem. Neurosci. 2023, 14, 159−169

sample. To evaluate the performance of classification model, sensitivity and specificity were calculated by the following equations:

$$\text{sensitivity} = \frac{\text{TP}}{(\text{TP} + \text{FN})} \times 100\% \quad (1)$$

$$\text{specificity} = \frac{\text{TN}}{(\text{TN} + \text{FP})} \times 100\% \quad (2)$$

True positive (TP) represents the proportion of the positive samples correctly identified as positive class. True negative (TN) refers to the proportion of negative samples correctly identified as negative class. False positive (FP) is the proportion of incorrectly identified positive samples into negative class, and false negative (FN) is the proportion of incorrectly identified negative samples into positive class. We used the equation "accuracy rate = 1 − class.error" to transfer class.error into the accuracy rate of RF model. Then, OOB value was used for an unbiased estimation of internal classification error to substitute the function of cross validation because OBB data were not involved in the model training. For neuron mapping and visualization, all 256 spectra were processed and input into the developed RF model for quality control, and all those satisfactorily meeting the classification were further extracted for visualization. For each group, the spectral number for visualization was around 200.

Statistical analysis was performed using SPSS 21.0, and all data were presented as the mean ± standard deviation (SD). Data of different classes were analyzed using one-way analysis of variance (ANOVA). Different small letters in each figure indicate significant difference (Duncan's test, $p < 0.05$) among groups ($n = 3$ for CK and SHAM groups; $n = 5$ for LFA, MFA, and HFA groups).

4. CONCLUSION

In this study, we conjunctively applied Raman biospectra, multivariate analysis, and random forest model to *in vitro* evaluate the levels of injury and intervention of neurons by ferulic acid in cerebral ischemia/reperfusion. Among several identified vibrational alterations representing the change of neuronal biomolecules, 1002 cm^{-1} representing phenylalanine was the most significant biomarker by all algorithms. Random forest model achieved satisfactory accuracy, sensitivity, and specificity to classify neuron viability and assess the neuroprotective effects of ferulic acid. The spectral phenylalanine-to-tryptophan ratio (1002−1614 cm^{-1}) was a reliable indicator to directly visualize the viability and neuroprotective effects of neurons. Our findings prove Raman spectroscopy coupled with multivariate analysis and machine learning is an ideal tool to distinguish the characteristic fingerprints in the cerebral ischemia reperfusion and offer potential clues for the precise assessment in pharmacological research like early stage diagnosis, drug screening, and intervention strategy optimization.

■ ASSOCIATED CONTENT

Supporting Information

The Supporting Information is available free of charge at https://pubs.acs.org/doi/10.1021/acschemneuro.2c00612.

Comparison of biochemical peaks with significant intensity changes among SHAM, HFA, and CK; significantly distinguished Raman alterations of neurons among different groups; PCA score plot of Raman spectra of neuroglia from different groups; cluster vectors of Raman spectra of neuroglia from different groups; Raman peak intensities of neuroglial cells among different groups; parameters associated with random forest model; main fingerprints of molecular assignments in neuron and neu according to references; detailed information on MeanDecreaseAccuracy and MeanDecreaseGini in the developed RF classification model (PDF)

■ AUTHOR INFORMATION

Corresponding Author

Dayi Zhang − *Key Laboratory of Groundwater Resources and Environment, Ministry of Education, Changchun 130021, P. R. China; College of New Energy and Environment, Jilin University, Changchun 130021, P. R. China*; Phone: +86(0) 10-62773232; Email: zhangdayi@tsinghua.org.cn

Authors

Mingying Liu − *School of Basic Medical Sciences, Zhejiang Chinese Medical University, Hangzhou 310053, P. R. China*; orcid.org/0000-0001-6261-8832

Ju Mu − *School of Basic Medical Sciences, Zhejiang Chinese Medical University, Hangzhou 310053, P. R. China*

Wan Gong − *School of Basic Medical Sciences, Zhejiang Chinese Medical University, Hangzhou 310053, P. R. China*

Kena Zhang − *School of Basic Medical Sciences, Zhejiang Chinese Medical University, Hangzhou 310053, P. R. China*

Maoyun Yuan − *School of Basic Medical Sciences, Zhejiang Chinese Medical University, Hangzhou 310053, P. R. China*

Yizhi Song − *CAS Key Laboratory of Bio-Medical Diagnostics, Suzhou Institute of Biomedical Engineering and Technology, Chinese Academy of Sciences, Suzhou 215163, P. R. China*; orcid.org/0000-0002-3005-382X

Bei Li − *State Key Laboratory of Applied Optics, Changchun Institute of Optics, Fine Mechanics and Physics, Chinese Academy of Sciences, Changchun 130033, P. R. China*

Naifu Jin − *College of Water Sciences, Beijing Normal University, Beijing 100875, P. R. China*

Wenjing Zhang − *Key Laboratory of Groundwater Resources and Environment, Ministry of Education, Changchun 130021, P. R. China; College of New Energy and Environment, Jilin University, Changchun 130021, P. R. China*

Complete contact information is available at: https://pubs.acs.org/10.1021/acschemneuro.2c00612

Author Contributions

[∞]M.L. and J.M. contributed equally to this work. M.L., W.G., and D.Z. designed the experiment. M.L., J.M., K.Z., and M.Y. did the experiments. M.L., J.M., Y.S., B.L., N.J., and W.Z. collected and analyzed the data. M.L. and D.Z. wrote the first draft of manuscript. M.L., J.M., and D.Z. revised the manuscript.

Notes

The authors declare no competing financial interest.

■ ACKNOWLEDGMENTS

This research was supported by the Research Project of Zhejiang Chinese Medical University (Grants 2021JKZKTS015B and 2021ZY11). D.Z. also acknowledges the support supplied by Chinese Government's Thousand Talents Plan for Young Professionals.

■ REFERENCES

(1) Kelly, P. J.; Kavanagh, E.; Murphy, S. Stroke: New Developments and Their Application in Clinical Practice. *Semin Neurol* **2016**, *36* (4), 317−23.

(2) Fisher, M.; Saver, J. L. Future directions of acute ischaemic stroke therapy. *Lancet Neurology* **2015**, *14* (7), 758−767.
(3) Shin, T. H.; Lee, D. Y.; Basith, S.; Manavalan, B.; Paik, M. J.; Rybinnik, I.; Mouradian, M. M.; Ahn, J. H.; Lee, G. Metabolome Changes in Cerebral Ischemia. *Cells* **2020**, *9* (7), 1630.
(4) Lim, S.; Kim, T. J.; Kim, Y. J.; Kim, C.; Ko, S. B.; Kim, B. S. Senolytic Therapy for Cerebral Ischemia-Reperfusion Injury. *Int. J. Mol. Sci.* **2021**, *22* (21), 11967.
(5) Franke, M.; Bieber, M.; Kraft, P.; Weber, A. N. R.; Stoll, G.; Schuhmann, M. K. The NLRP3 inflammasome drives inflammation in ischemia/reperfusion injury after transient middle cerebral artery occlusion in mice. *Brain Behav. Immunity* **2021**, *92*, 221−231.
(6) Mhillaj, E.; Catino, S.; Miceli, F. M.; Santangelo, R.; Trabace, L.; Cuomo, V.; Mancuso, C. Ferulic Acid Improves Cognitive Skills Through the Activation of the Heme Oxygenase System in the Rat. *Mol. Neurobiol* **2018**, *55* (2), 905−916.
(7) Zhang, Q.; Zhao, Y.; Xu, Y.; Chen, Z.; Liu, N.; Ke, C.; Liu, B.; Wu, W. Sodium ferulate and n-butylidenephthalate combined with bone marrow stromal cells (BMSCs) improve the therapeutic effects of angiogenesis and neurogenesis after rat focal cerebral ischemia. *J. Transl. Med.* **2016**, *14* (1), 223.
(8) Zhou, P.; Du, S.; Zhou, L.; Sun, Z.; Zhuo, L. H.; He, G.; Zhao, Y.; Wu, Y.; Zhang, X. Tetramethylpyrazine2′Osodium ferulate provides neuroprotection against neuroinflammation and brain injury in MCAO/R rats by suppressing TLR-4/NF-kappaB signaling pathway. *Pharmacol., Biochem. Behav.* **2019**, *176*, 33−42.
(9) Jin, Y.; Yan, E. Z.; Fan, Y.; Guo, X. L.; Zhao, Y. J.; Zong, Z. H.; Liu, Z. Neuroprotection by sodium ferulate against glutamate-induced apoptosis is mediated by ERK and PI3 kinase pathways. *Acta Pharmacol Sin* **2007**, *28* (12), 1881−90.
(10) Joshi, G.; Perluigi, M.; Sultana, R.; Agrippino, R.; Calabrese, V.; Butterfield, D. A. In vivo protection of synaptosomes by ferulic acid ethyl ester (FAEE) from oxidative stress mediated by 2,2-azobis(2-amidino-propane)dihydrochloride (AAPH) or Fe(2+)/H(2)O(2): insight into mechanisms of neuroprotection and relevance to oxidative stress-related neurodegenerative disorders. *Neurochem. Int.* **2006**, *48* (4), 318−27.
(11) Catino, S.; Paciello, F.; Miceli, F.; Rolesi, R.; Troiani, D.; Calabrese, V.; Santangelo, R.; Mancuso, C. Ferulic Acid Regulates the Nrf2/Heme Oxygenase-1 System and Counteracts Trimethyltin-Induced Neuronal Damage in the Human Neuroblastoma Cell Line SH-SY5Y. *Front. Pharmacol.* **2016**, *6*, 305.
(12) Mhillaj, E.; Cuomo, V.; Trabace, L.; Mancuso, C. The Heme Oxygenase/Biliverdin Reductase System as Effector of the Neuroprotective Outcomes of Herb-Based Nutritional Supplements. *Front. Pharmacol.* **2019**, *10*, 1298.
(13) Ren, Z.; Zhang, R.; Li, Y.; Li, Y.; Yang, Z.; Yang, H. Ferulic acid exerts neuroprotective effects against cerebral ischemia/reperfusion-induced injury via antioxidant and anti-apoptotic mechanisms in vitro and in vivo. *Int. J. Mol. Med.* **2017**, *40* (5), 1444−1456.
(14) Han, Y.; Chen, Y.; Zhang, Q.; Liu, B. W.; Yang, L.; Xu, Y. H.; Zhao, Y. H. Overview of therapeutic potentiality of Angelica sinensis for ischemic stroke. *Phytomedicine* **2021**, *90*, 153652.
(15) Tsutsumi, Y. Pitfalls and Caveats in Applying Chromogenic Immunostaining to Histopathological Diagnosis. *Cells* **2021**, *10* (6), 1501.
(16) Fischer, A. H.; Jacobson, K. A.; Rose, J.; Zeller, R. Hematoxylin and eosin staining of tissue and cell sections. *Cold Spring Harbor Protoc* **2008**, *2008*, pdb.prot4986.
(17) Feldman, A. T.; Wolfe, D. Tissue processing and hematoxylin and eosin staining. *Methods Mol. Biol.* **2014**, *1180*, 31−43.
(18) Pence, I.; Mahadevan-Jansen, A. Clinical instrumentation and applications of Raman spectroscopy. *Chem. Soc. Rev.* **2016**, *45* (7), 1958−79.
(19) Paraskevaidi, M.; Morais, C. L. M.; Halliwell, D. E.; Mann, D. M. A.; Allsop, D.; Martin-Hirsch, P. L.; Martin, F. L. Raman Spectroscopy to Diagnose Alzheimer's Disease and Dementia with Lewy Bodies in Blood. *ACS Chem. Neurosci.* **2018**, *9* (11), 2786−2794.
(20) Traynor, D.; Behl, I.; O'Dea, D.; Bonnier, F.; Nicholson, S.; O'Connell, F.; Maguire, A.; Flint, S.; Galvin, S.; Healy, C. M.; Martin, C. M.; O'Leary, J. J.; Malkin, A.; Byrne, H. J.; Lyng, F. M. Raman spectral cytopathology for cancer diagnostic applications. *Nat. Protoc* **2021**, *16* (7), 3716−3735.
(21) Yu, B.; Ge, M.; Li, P.; Xie, Q.; Yang, L. Development of surface-enhanced Raman spectroscopy application for determination of illicit drugs: Towards a practical sensor. *Talanta* **2019**, *191*, 1−10.
(22) Fonseca, E. A.; Lafeta, L.; Cunha, R.; Miranda, H.; Campos, J.; Medeiros, H. G.; Romano-Silva, M. A.; Silva, R. A.; Barbosa, A. S.; Vieira, R. P.; Malard, L. M.; Jorio, A. A fingerprint of amyloid plaques in a bitransgenic animal model of Alzheimer's disease obtained by statistical unmixing analysis of hyperspectral Raman data. *Analyst* **2019**, *144* (23), 7049−7056.
(23) Cook, A. M.; Morgan Jones, G.; Hawryluk, G. W. J.; Mailloux, P.; McLaughlin, D.; Papangelou, A.; Samuel, S.; Tokumaru, S.; Venkatasubramanian, C.; Zacko, C.; Zimmermann, L. L.; Hirsch, K.; Shutter, L. Guidelines for the Acute Treatment of Cerebral Edema in Neurocritical Care Patients. *Neurocrit Care* **2020**, *32* (3), 647−666.
(24) Chamorro, Á.; Dirnagl, U.; Urra, X.; Planas, A. M. Neuroprotection in acute stroke: targeting excitotoxicity, oxidative and nitrosative stress, and inflammation. *Lancet Neurology* **2016**, *15* (8), 869−881.
(25) Thomalla, G.; Boutitie, F.; Ma, H.; Koga, M.; Ringleb, P.; Schwamm, L. H.; Wu, O.; Bendszus, M.; Bladin, C. F.; Campbell, B. C. V.; Cheng, B.; Churilov, L.; Ebinger, M.; Endres, M.; Fiebach, J. B.; Fukuda-Doi, M.; Inoue, M.; Kleinig, T. J.; Latour, L. L.; Lemmens, R.; Levi, C. R.; Leys, D.; Miwa, K.; Molina, C. A.; Muir, K. W.; Nighoghossian, N.; Parsons, M. W.; Pedraza, S.; Schellinger, P. D.; Schwab, S.; Simonsen, C. Z.; Song, S. S.; Thijs, V.; Toni, D.; Hsu, C. Y.; Wahlgren, N.; Yamamoto, H.; Yassi, N.; Yoshimura, S.; Warach, S.; Hacke, W.; Toyoda, K.; Donnan, G. A.; Davis, S. M.; Gerloff, C. Intravenous alteplase for stroke with unknown time of onset guided by advanced imaging: systematic review and meta-analysis of individual patient data. *Lancet* **2020**, *396*, 1574.
(26) Li, H.; Luo, Y.; Liu, P.; Liu, P.; Hua, W.; Zhang, Y.; Zhang, L.; Li, Z.; Xing, P.; Zhang, Y.; Hong, B.; Yang, P.; Liu, J. Exosomes containing miR-451a is involved in the protective effect of cerebral ischemic preconditioning against cerebral ischemia and reperfusion injury. *CNS Neurosci Ther* **2021**, *27* (5), 564−576.
(27) Lin, T.; Song, Y. L.; Liao, J.; Liu, F.; Zeng, T. T. Applications of surface-enhanced Raman spectroscopy in detection fields. *Nanomedicine* **2020**, *15* (7), 2971−2989.
(28) Dutta, A.; Gautam, R.; Chatterjee, S.; Ariese, F.; Sikdar, S. K.; Umapathy, S. Ascorbate protects neurons against oxidative stress—A raman microspectroscopic study. *ACS Chem. Neurosci.* **2015**, *6* (11), 1794−1801.
(29) Bian, Z.; Furuya, N.; Zheng, D. M.; Trejo, J.; Tada, N.; Ezaki, J.; Ueno, T. Ferulic acid induces mammalian target of rapamycin inactivation in cultured mammalian cells. *Biol. Pharm. Bull.* **2013**, *36* (1), 120.
(30) Barth, A.; Zscherp, C. What vibrations tell us about proteins. *Q. Rev. Biophys.* **2002**, *35* (4), 369−430.
(31) Rygula, A.; Majzner, K.; Marzec, K. M.; Kaczor, A.; Pilarczyk, M.; Baranska, M. Raman spectroscopy of proteins: a review. *J. Raman Spectrosc.* **2013**, *44* (8), 1061−1076.
(32) Hochrainer, K. Protein Modifications with Ubiquitin as Response to Cerebral Ischemia-Reperfusion Injury. *Transl Stroke Res.* **2018**, *9* (2), 157−173.
(33) Cui, Y.; Liu, X.; Li, X.; Yang, H. In-Depth Proteomic Analysis of the Hippocampus in a Rat Model after Cerebral Ischaemic Injury and Repair by Danhong Injection (DHI). *Int. J. Mol. Sci.* **2017**, *18* (7), 1355.
(34) Kahl, A.; Blanco, I.; Jackman, K.; Baskar, J.; Milaganur Mohan, H.; Rodney-Sandy, R.; Zhang, S.; Iadecola, C.; Hochrainer, K. Cerebral ischemia induces the aggregation of proteins linked to neurodegenerative diseases. *Sci. Rep.* **2018**, *8* (1), 2701.
(35) Lin, S.; Zhou, G.; Shao, W.; Fu, Z. Impact of dexmedetomidine on amino acid contents and the cerebral ultrastructure of rats with

cerebral ischemia-reperfusion injury. *Acta Cir. Bras.* **2017**, *32* (6), 459−466.
(36) Cheng, X.; Yang, Y. L.; Li, W. H.; Liu, M.; Wang, Y. H.; Du, G. H. Cerebral ischemia-reperfusion aggravated cerebral infarction injury and possible differential genes identified by RNA-Seq in rats. *Brain Res. Bull.* **2020**, *156*, 33−42.
(37) Yi, D.; Wang, Q.; Zhao, Y.; Song, Y.; You, H.; Wang, J.; Liu, R.; Shi, Z.; Chen, X.; Luo, Q. Alteration of N (6) -Methyladenosine mRNA Methylation in a Rat Model of Cerebral Ischemia-Reperfusion Injury. *Front Neurosci* **2021**, *15*, 605654.
(38) Roy, D.; Tedeschi, A. The Role of Lipids, Lipid Metabolism and Ectopic Lipid Accumulation in Axon Growth, Regeneration and Repair after CNS Injury and Disease. *Cells* **2021**, *10* (5), 1078.
(39) Fernstrom, J. D.; Fernstrom, M. H. Tyrosine, phenylalanine, and catecholamine synthesis and function in the brain. *J. Nutr.* **2007**, *137*, 1539S−1547S.
(40) Kimberly, W. T.; Wang, Y.; Pham, L.; Furie, K. L.; Gerszten, R. E. Metabolite profiling identifies a branched chain amino acid signature in acute cardioembolic stroke. *Stroke* **2013**, *44* (5), 1389−95.
(41) Kamtchum-Tatuene, J.; Jickling, G. C. Blood Biomarkers for Stroke Diagnosis and Management. *Neuromolecular Med.* **2019**, *21* (4), 344−368.
(42) Qi, B.; Zhang, Y. Y.; Xu, B.; Zhang, Y. H.; Fei, G. Q.; Lin, L.; Li, Q. P. Metabolomic Characterization of Acute Ischemic Stroke Facilitates Metabolomic Biomarker Discovery. *Appl. Biochem. Biotechnol.* **2022**, *194* (11), 5443−5455.
(43) Xu, J.; Liu, X.; Luo, L.; Tang, L.; Guo, N.; Liu, M.; Li, H.; Zhang, F.; Zhang, Y.; Li, D.; Zhao, Y.; Wu, H.; Yang, H. A Metabonomics Investigation into the Therapeutic Effects of BuChang NaoXinTong Capsules on Reversing the Amino Acid-Protein Interaction Network of Cerebral Ischemia. *Oxid. Med. Cell. Longevity* **2019**, *2019*, 7258624.
(44) Chistiakov, D. A.; Shkurat, T. P.; Melnichenko, A. A.; Grechko, A. V.; Orekhov, A. N. The role of mitochondrial dysfunction in cardiovascular disease: a brief review. *Ann. Med.* **2018**, *50* (2), 121−127.
(45) Orellana-Urzua, S.; Rojas, I.; Libano, L.; Rodrigo, R. Pathophysiology of Ischemic Stroke: Role of Oxidative Stress. *Curr. Pharm. Des* **2020**, *26* (34), 4246−4260.
(46) He, H.; Yan, S.; Lyu, D.; Xu, M.; Ye, R.; Zheng, P.; Lu, X.; Wang, L.; Ren, B. Deep Learning for Biospectroscopy and Biospectral Imaging: State- of-the-Art and Perspectives. *Anal. Chem.* **2021**, *93* (8), 3653−3665.
(47) Durrant, B.; Trappett, M.; Shipp, D.; Notingher, I. Recent developments in spontaneous Raman imaging of living biological cells. *Curr. Opin. Chem. Biol.* **2019**, *51*, 138−145.
(48) Pezzotti, G.; Horiguchi, S.; Boschetto, F.; Adachi, T.; Marin, E.; Zhu, W.; Yamamoto, T.; Kanamura, N.; Ohgitani, E.; Mazda, O. Raman Imaging of Individual Membrane Lipids and Deoxynucleoside Triphosphates in Living Neuronal Cells during Neurite Outgrowth. *ACS Chem. Neurosci.* **2018**, *9* (12), 3038−3048.
(49) Kochan, K.; Peng, H. D.; Gwee, E. S. H.; Izgorodina, E.; Haritos, V.; Wood, B. R. Raman spectroscopy as a tool for tracking cyclopropane fatty acids in genetically engineered Saccharomyces cerevisiae. *Analyst* **2019**, *144* (3), 901−912.
(50) Perez-Guaita, D.; Kochan, K.; Martin, M.; Andrew, D. W.; Heraud, P.; Richards, J. S.; Wood, S. R. Multimodal vibrational imaging of cells. *Vib. Spectrosc.* **2017**, *91*, 46−58.
(51) Chen, X.; Liu, Y.; Zhu, J.; Lei, S.; Dong, Y.; Li, L.; Jiang, B.; Tan, L.; Wu, J.; Yu, S.; Zhao, Y. GSK-3beta downregulates Nrf2 in cultured cortical neurons and in a rat model of cerebral ischemia-reperfusion. *Sci. Rep.* **2016**, *6*, 20196.
(52) Longa, E. Z.; Weinstein, P. R.; Carlson, S.; Cummins, R. Reversible middle cerebral artery occlusion without craniectomy in rats. *Stroke* **1989**, *20* (1), 84−91.
(53) Butler, H. J.; Ashton, L.; Bird, B.; Cinque, G.; Curtis, K.; Dorney, J.; Esmonde-White, K.; Fullwood, N. J.; Gardner, B.; Martin-Hirsch, P. L.; Walsh, M. J.; McAinsh, M. R.; Stone, N.; Martin, F. L. Using Raman spectroscopy to characterize biological materials. *Nat. Protoc.* **2016**, *11* (4), 664−687.
(54) Trevisan, J.; Angelov, P. P.; Scott, A. D.; Carmichael, P. L.; Martin, F. L. IRootLab: a free and open-source MATLAB toolbox for vibrational biospectroscopy data analysis. *Bioinformatics* **2013**, *29* (8), 1095−1097.